

## Evidence of interfacial charge trapping mechanism in polyaniline/reduced graphene oxide nanocomposites

Rakibul Islam, Anthony N. Papathanassiou, Roch Chan Yu King, Jean-François Brun, and Frederick Rousset

Citation: [Applied Physics Letters](#) **107**, 053102 (2015); doi: 10.1063/1.4927591

View online: <http://dx.doi.org/10.1063/1.4927591>

View Table of Contents: <http://scitation.aip.org/content/aip/journal/apl/107/5?ver=pdfcov>

Published by the [AIP Publishing](#)

---

### Articles you may be interested in

[Multilayered graphene acquires ferromagnetism in proximity with magnetite particles](#)

*Appl. Phys. Lett.* **106**, 212401 (2015); 10.1063/1.4921770

[Synthesis of ZnO decorated graphene nanocomposite for enhanced photocatalytic properties](#)

*J. Appl. Phys.* **115**, 173504 (2014); 10.1063/1.4874877

[Dielectric property of NiTiO<sub>3</sub> doped substituted ortho-chloropolyaniline composites](#)

*AIP Advances* **3**, 112113 (2013); 10.1063/1.4832223

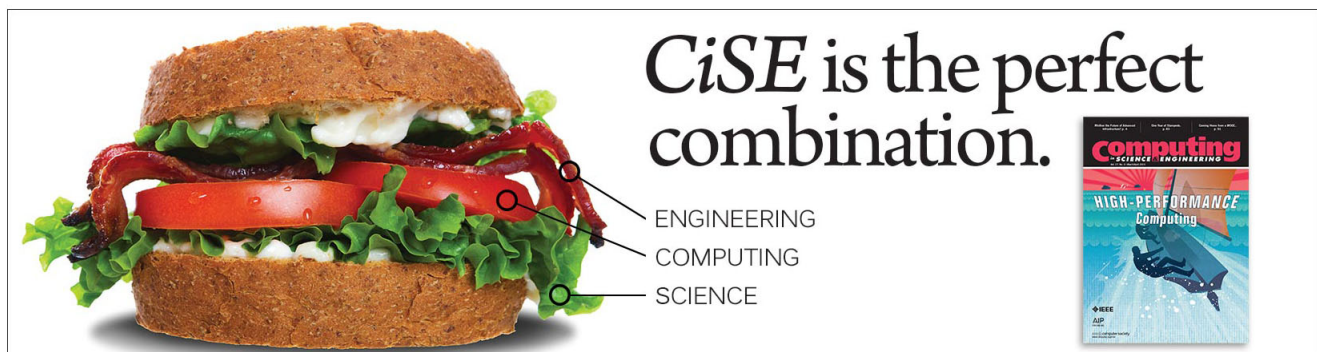
[Influence of Cr<sub>2</sub>O<sub>3</sub> nanoparticles on the physical properties of polyvinyl alcohol](#)

*J. Appl. Phys.* **112**, 093525 (2012); 10.1063/1.4764864

[Theoretical and experimental approach on dielectric properties of ZnO nanoparticles and polyurethane/ZnO nanocomposites](#)

*J. Appl. Phys.* **112**, 054106 (2012); 10.1063/1.4749414

---

An advertisement for CiSE (Computing, Science, Engineering). On the left is a large sandwich with lettuce, tomato, and meat. On the right is the cover of the journal 'Computing: Science, Engineering, and Technology' with the headline 'HIGH-PERFORMANCE Computing'. The text 'CiSE is the perfect combination.' is written in a large, serif font. Below this text, three lines of text are listed: 'ENGINEERING', 'COMPUTING', and 'SCIENCE'. Three lines with circular endpoints point from these text elements to the sandwich, suggesting that the sandwich is a metaphor for the combination of these three fields.

## Evidence of interfacial charge trapping mechanism in polyaniline/reduced graphene oxide nanocomposites

Rakibul Islam,<sup>1,2</sup> Anthony N. Papathanassiou,<sup>3</sup> Roch Chan Yu King,<sup>4</sup> Jean-François Brun,<sup>1,2</sup> and Frederick Roussel<sup>1,2,a)</sup>

<sup>1</sup>University of Lille, Sciences & Technologies, Unité Matériaux et Transformations (UMET), UMR CNRS 8207, U.F.R. de Physique, P5, 59655 Villeneuve d'Ascq Cedex, France

<sup>2</sup>COMUE Lille Nord de France, BP 50458-59658 Villeneuve d'Ascq Cedex, France

<sup>3</sup>Physics Department, Solid State Physics Section, University of Athens, Panepistimiopolis, GR15784 Zografos, Athens, Greece

<sup>4</sup>Science Division, University of Science and Arts of Oklahoma, Chickasha, Oklahoma 73018, USA

(Received 11 June 2015; accepted 17 July 2015; published online 3 August 2015)

Relaxation mechanisms in polyaniline (PANI)/Reduced Graphene Oxide (RGO) nanocomposites are investigated using broad band dielectric spectroscopy. The multilayered nanostructural features of the composites and the intimate interactions between PANI and RGO are evidenced by field emission scanning electron microscopy, transmission electron microscopy, and Raman spectroscopy. Increasing the RGO fraction in the composites results in a relaxation process observed at a frequency of ca. 5 kHz. This mechanism is associated with an electrical charge trapping phenomenon occurring at the PANI/RGO interfaces. The dielectric relaxation processes are interpreted according to the Sillars approach and the results are consistent with the presence of conducting prolate spheroids (RGO) embedded into a polymeric matrix (PANI). Dielectric permittivity data are analyzed within the framework of the Kohlrausch-William-Watts model, evidencing a Debye-like relaxation process. © 2015 AIP Publishing LLC.

[<http://dx.doi.org/10.1063/1.4927591>]

Graphene based polymer-nanocomposites have been the subject of intensive research in recent years due to their numerous promising technical applications such as thermal management equipments, reinforced mechanical systems, or electronic components.<sup>1–5</sup> More advanced applications focus on the charge trapping capability of graphene-based nanocomposites for the design and fabrication of EMI shielding devices, supercapacitors, or memory devices for portable electronics.<sup>6–8</sup> Performance of these systems rely on the interactions between the carbonaceous nanostructure and its host, the quality of the filler dispersion, or the aspect ratio of graphene layers. These crucial parameters strongly impact the physical properties of the hybrid materials. Numerous works have been conducted to highlight the influence of the filler fraction on the electrical and thermal properties of the nanocomposites. While thermal transport is usually limited by phonon scattering at the filler/host interface, electrical charge transport has been described by 2D or 3D percolation mechanisms.<sup>9,10</sup> To explain these various types of transport processes, interfacial phenomena between the filler and the host are usually evoked but further investigations are required to characterize and explain the physical mechanisms occurring at the nanoscale level.

In the present letter, Broadband Dielectric Spectroscopy (BDS) was employed to investigate the electric and dielectric properties of polyaniline/reduced graphene oxide (PANI/RGO) nanocomposites with various RGO weight fractions. In particular, electric charge transport is explored from frequency dependent AC conductivity measurements providing interesting insights into the relaxation mechanisms, which

take place in the nanohybrids at various spatio-temporal scales. Dielectric permittivity data are analyzed within the framework of the Kohlrausch-William-Watts (KWW) model. Raman spectroscopy, Field Emission Scanning Electron Microscopy (FE-SEM), and Transmission Electron Microscopy (TEM) investigations are also reported to determine the structural and morphological features of the materials. The relationship between the morphology and the charge localization within the composites is also studied and discussed according to existing models.

PANI/RGO hybrids were *in situ* chemically synthesized based on a procedure reported elsewhere.<sup>11</sup> The weight fraction of RGO in the composites was varied from 0 to 15 wt. %. The PANI/RGO pellets were prepared from grinded, as-produced materials by cold pressing (450 MPa) providing test samples with a diameter of 12.8 mm and a thickness of ca.  $290 \pm 20 \mu\text{m}$ . The as-prepared pellets were placed between aluminium electrodes for dielectric investigations. Impedance measurements were carried out at room temperature ( $T \approx 20^\circ\text{C}$ ) on a Modulab-MTS test system (Solarton Analytical—Ametek) in the frequency range of 10 mHz–1 MHz; the amplitude of the oscillating voltage was set to 100 mV. Dielectric data were fitted using the Grafty software.<sup>12</sup> Morphological and structural characteristics of PANI/RGO composites were investigated by FE-SEM (Hitachi S4700 operating at 6 kV) and TEM (FEI Tecnai G2 operating at 20 kV). Raman spectroscopy analyses were performed with a Horiba Jobin Yvon Labram HR operating with a HeNe laser ( $\lambda = 632.8 \text{ nm}$  and  $P = 0.1 \text{ mW}$ ); spectra were fitted using the freely available software FOCUS.<sup>13</sup>

A typical Raman spectrum of PANI-RGO composites is presented in Figure 1(a). The characteristic bands of the

<sup>a)</sup>Electronic mail: frederick.roussel@univ-lille1.fr

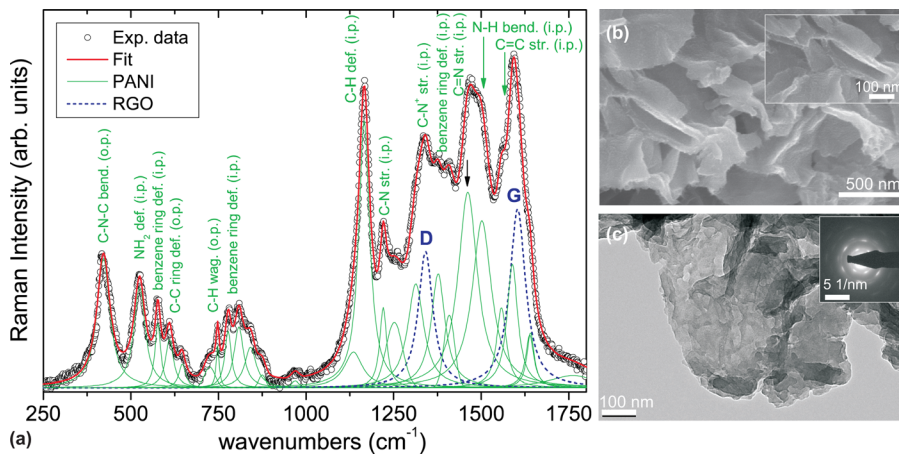


FIG. 1. (a) Raman spectrum of the PANI/RGO nanocomposite containing 10 wt. % RGO. (b) SEM and (c) TEM images showing the morphology and structure of the corresponding PANI/RGO hybrid; inset of (c): electron diffraction pattern of the platelet observed by TEM.

doped polymer were found to be in good agreement with those reported in the literature confirming the presence of polyaniline.<sup>14,15</sup> The two bands at 1347 and 1597  $\text{cm}^{-1}$  were assigned to the D band (disorder-induced band) and the G band (in-plane stretching mode) of RGO, respectively.<sup>9,16</sup> The characteristic Raman bands of each component demonstrate that RGO-reinforced PANI nanocomposites have been effectively prepared. The intense vibration mode at 1460  $\text{cm}^{-1}$  (C=N quinoid stretching) evidences that RGO favors the quinoid form of PANI. This result shows that physical interactions between the basal planes of RGO and quinoid rings of PANI are strongly promoted by  $\pi-\pi$  stacking and are consistent with the observations of the previous works.<sup>11,15,17</sup> Figures 1(b) and 1(c) display the FE-SEM and TEM images of PANI-RGO composites with 10 wt. % RGO. Microscopy observations reveal that graphene sheets are covered with a PANI layer resulting in a lamellar morphology. The electron diffraction pattern (Inset of Fig. 1(c)) shows six fold symmetric diffraction points confirming the hexagonal crystalline structure of the graphitic planes of RGO. Structural disorder of composites is also evident from the lattice fringe patterns which can be associated with the structural signatures of semi-crystalline PANI and multilayered graphenes.

The real part of the complex electrical conductivity  $\sigma^* = \sigma' + j\sigma''$  is related to the imaginary part of the complex permittivity  $\epsilon^* = \epsilon' + j\epsilon''$  through the relation  $\sigma' = 2\pi f \epsilon_0 \epsilon''$  or  $\epsilon'' = \frac{\sigma'}{2\pi f \epsilon_0} \propto \frac{G(f)}{f}$ ,<sup>18,19</sup> where  $f$  denotes the frequency of the harmonic voltage applied to the sample,  $\epsilon_0$  is the permittivity of free space, and  $G(f)$  is the measured conductance. The frequency dependence of  $\epsilon''$  experimental data for pure PANI and representative nanocomposites are displayed in Figure 2(a). A relaxation process is detected in the range of  $10^3-10^4$  Hz for nanocomposites, but not for pure PANI, indicating that this process must be associated with the presence of RGO in the materials. In the MHz region, an additional relaxation mechanism is partially observed in the vicinity of the detection limit of our impedance analyzer and is beyond the scope of the present work. In order to completely characterize the dielectric spectra, a quantitative analysis of experimental data were carried out using a function

$$\epsilon''(f) = \epsilon_1''(f) + \epsilon_2''(f), \quad (1)$$

composed of a DC conductivity term

$$\epsilon_1''(f) = \frac{\sigma_{DC}}{\epsilon_0 (2\pi f)^n}, \quad (2)$$

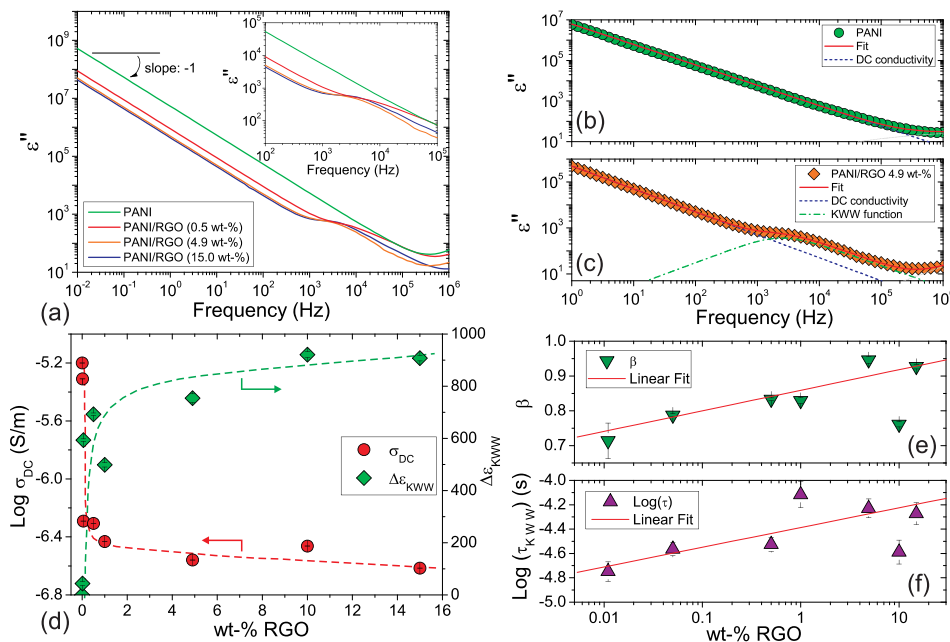


FIG. 2. (a) Imaginary part  $\epsilon''$  of the complex dielectric permittivity versus frequency  $f$  for pure PANI and composites containing 0.5, 4.9, and 15.0 wt. % RGO. Inset: enlarged view of the relaxation process observed around  $10^3$  Hz. (b) and (c)  $\epsilon''$  vs.  $f$  for pure PANI and PANI/RGO (4.9 wt. %), respectively: symbols are experimental data point, whereas lines are the best fitting curves to Eq. (1). Dependence of fitting parameters on RGO loading: (d) DC conductivity  $\sigma_{DC}$  and intensity of the KWW relaxation peak  $\Delta\epsilon_{KWW}$ , (e) stretching exponent  $\beta$ , and (f) relaxation time of the KWW peak  $\tau_{KWW}$ .

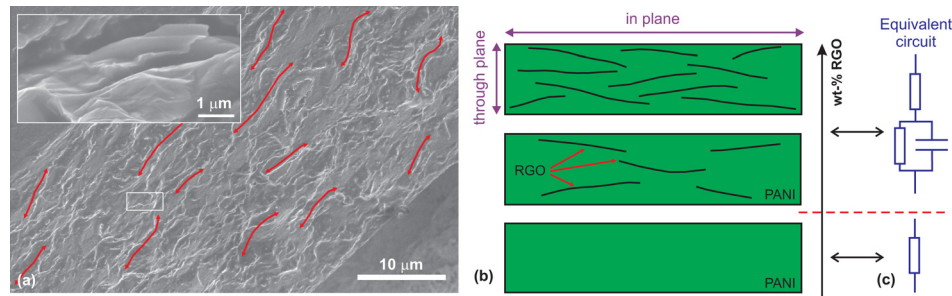


FIG. 3. (a) Cross sectional SEM view of PANI/RGO pressed pellet (1.1 wt. % RGO). Red arrows illustrate the main orientation of layered platelets; the inset displays the enlarged area of the white rectangle showing PANI-wrapped RGO platelets. (b) Schematic view of pellet cross sections starting from pure PANI (bottom) to higher RGO loadings (top) and (c) proposed schematic equivalent circuits according to dielectric behaviors.

and  $\epsilon_2''(f)$ , which is the Fourier transform of the KWW stretched exponential functions<sup>20,21</sup>

$$\epsilon_2''(t) = \Delta\epsilon_{KWW} \exp\left(\frac{-t}{\tau_{KWW}}\right)^\beta \quad (3)$$

where  $\Delta\epsilon_{KWW}$  is the relaxation strength,  $\tau_{KWW}$  is the KWW-relaxation time, and  $\beta$  is the stretching exponent ( $0 < \beta \leq 1$ ). Figures 2(b) and 2(c) show the frequency dependence of  $\epsilon''$  experimental data (symbols) and fitting curves (solid and dashed lines) for pure PANI and a representative sample of PANI/RGO nanocomposite (4.9 wt. %). For pure PANI, all data points lie on a straight line with a slope of  $-1$  which is attributed to the DC conductivity term (Fig. 2(b), dashed line). This statement is also valid for nanocomposites up to  $f = 5 \times 10^2$  Hz above which an additional dielectric relaxation peak is observed. This peak can be fitted with a KWW function (Fig. 2(c), dashed-dotted line) demonstrating that a very good matching is obtained between the experimental data and the fitting curves retrieved from Eq. (1).

Figure 2(d) shows that the DC conductivity ( $\sigma_{DC}$ ) decreases with increasing RGO fraction. This behavior is unexpected because a notable enhancement of percolation process is usually observed for graphene-based nanocomposites.<sup>9,10</sup> A possible explanation of this finding could come from the sample pelletization process which might favor a parallel arrangement of PANI/RGO platelets as shown in Figure 3(a) by SEM and cartooned in Fig. 3(b). Recalling that PANI/RGO composites were prepared by *in-situ* chemical synthesis, RGO acts as a seed for PANI growth, i.e., the surfaces of RGO platelets are fully covered with a layer of PANI forming a core(RGO)/shell(PANI) structure. Due to their planar 2D shape, PANI/RGO platelets are most likely stacked in a parallel manner during compression leading to a layered-like morphology where physical contacts/connections between platelets occurred through their PANI shells. This geometrical arrangement of PANI/RGO platelets is supported by the previous reports where graphene platelets preferentially lie parallel to each other inducing anisotropic transport properties.<sup>22,23</sup> In such a morphology, PANI/RGO platelets can be electrically assimilated to leaky capacitors assembled in a series of parallel Resistance-Capacitor (RC) components as proposed in Fig. 3(c). This system models a Debye-like relaxation process, which can be used to describe the dielectric loss observed in Fig. 2.

It should be also pointed out that the charge motion/transfer is strongly dependent on the filler (RGO)/host (PANI)

interface.<sup>11,17</sup> In this layered-like core/shell structure, electric charges are trapped due to uneven electrical conductivity between PANI and RGO. With increasing fraction of RGO, the number of interfaces in the nanocomposite increases, which act as trapping centers for charge carriers. The planar 2D shape of PANI/RGO platelets combined with their parallel assembly favors the *in plane* charge motion along the basal planes of RGO, while the *through plane* flow is impeded by filler/host interfaces. This leads to anisotropic electric transport which is reflected by a lower *through plane* (volume) conductivity as measured by impedance spectroscopy compared to that of the *in plane* (surface) value retrieved from sheet resistivity measurements using the 4-point collinear probe technique.<sup>11</sup> Thus, on increasing the RGO content, interfaces hinder the *through plane* charge motion, which induces percolation network changes, i.e., fewer pathways are available for carriers to move macroscopically, while charged clusters bounded at interfaces permit mainly short range electric charge flow. These clusters reduce the number of mobile charges (decrease of  $\sigma_{DC}$  values) and induce capacitance effects due to charge trapping. The increase of the KWW peak intensity ( $\Delta\epsilon_{KWW}$ ) as a function of RGO content (Fig. 2(d)) corroborates with the conductivity data. The results are also in good agreement with and can be described by the interfacial polarization model proposed by Sillars<sup>24</sup> for low concentration of conducting oblate spheroid inclusions (RGO) embedded in a matrix (PANI). In this model, the intensity of the interfacial polarization is dependent on the volume fraction of filler ( $v_{RGO}$ ) as follows:<sup>24</sup>  $\Delta\epsilon = v_{RGO} \frac{\epsilon_{PANI}^2}{\epsilon_{RGO}}$ , which complies with the observed RGO fraction dependence of  $\Delta\epsilon_{KWW}$  in PANI/RGO nanocomposites.

The stretching component  $\beta$  characteristic and relaxation time  $\tau_{KWW}$  retrieved from the KWW function are increased with RGO fraction (Figs. 2(e) and 2(f)).  $\beta$  approaches the value 1, which is typical of a Debye-like relaxation. In order to get further insights into this process, the *mean dielectric relaxation time*  $\langle\tau\rangle$  is calculated with the relation  $\langle\tau\rangle = \left(\frac{\tau_{KWW}}{\beta}\right) \Gamma(\beta^{-1})$  (Ref. 25) which provided a mean value of  $\langle\tau\rangle \approx 6.3 \times 10^{-5}$  s for all nanocomposites. In addition, the relaxation time of dielectric losses, i.e., the inverse of the relaxation maximum frequency, is found to be  $\tau_{max} = f_{max}^{-1} \approx 2.5 \times 10^{-4}$  s and is also roughly insensitive to the increase of RGO fraction. In other words, the relaxation time-scale is practically constant; subsequently, the characteristic scale which is, to a first approximation, proportional to reciprocal relaxation time, is invariant to increased RGO

content. Since the relaxation time is proportional to the time required for a trapped charge to move along a platelet, a constant value of  $\tau_{max}$  indicates that PANI/RGO platelets are of similar dimensions for all composites. The result is consistent with the previous morphological investigations performed by SEM which demonstrated that the dimensions of the RGO platelets when covered with PANI do not change significantly with increasing RGO loading.<sup>11</sup> This is further supported by the Sillars model which predicts that the relaxation time  $\tau = \epsilon_0 \frac{\epsilon_{RGO}}{\sigma_{RGO}}$  (Ref. 24) is unaffected by the fraction of the conducting oblate spheroid inclusions.

It should be also mentioned that relaxation mechanisms may arise from the disorder present in semi-conducting materials. This phenomenon can be verified with the use of the Barton-Nakajima-Namikawa (BNN) relation:<sup>26</sup>  $\sigma_{DC} = 2\pi f_{max} \epsilon_0 p \Delta \epsilon$ , where  $p$  is a constant on the order of unity and  $\Delta \epsilon$  is the relaxation strength. In the present study,  $f_{max}$  was found to be roughly constant which implies, according to the BNN equation, that  $\sigma_{DC} \propto \Delta \epsilon$ . The latter finding is in contradiction with the experimental observations in which the DC conductivity decreases and the intensity of the dielectric relaxation increases with increasing RGO fraction (Fig. 2(d)). Hence, the BNN relation is not fulfilled, i.e., the observed relaxation peak can hardly be attributed to relaxation within the PANI phase. In addition, if the observed relaxation originated from disorder in the PANI rich phase, fitting parameters  $\tau_{KWW}$  and  $\beta$  would be independent of RGO loading which is obviously not the case as shown in Figs. 2(e) and 2(f).

In summary, the structural and electric properties of a series of PANI/RGO nanocomposites are investigated. The layered-like morphology of the composites favors an electrical charge trapping phenomenon occurring at the PANI/RGO interfaces with increasing RGO fraction. This phenomenon leads to a relaxation process observed at a frequency of ca. 5 kHz and is interpreted according to the Sillars approach, i.e., the results are consistent with the presence of conducting prolate spheroids (RGO) embedded into a polymeric matrix (PANI). Dielectric permittivity data are analyzed within the framework of the KWW model evidencing a Debye-like relaxation process. This suggests that PANI/RGO platelets can be electrically assimilated to an assembly of parallel RC components. Such composite materials exhibiting charge trapping capabilities may find promising applications in supercapacitors or gate memory devices.

A.P. acknowledges the University of Lille for inviting him as a Visiting Professor. R.C.Y.K thanks the Emerson fund and the University of Lille for financial support. SEM and TEM experiments were performed at the *Centre Commun de Microscopie (CCM)* of the University of Lille. Dr. Ahmed Addad is kindly acknowledged for his help with TEM. The authors are indebted to Dr. M. Moreau for providing access to the LASIR Raman facilities.

<sup>1</sup>K. M. F. Shahil and A. A. Balandin, "Graphene—Multilayer graphene nanocomposites as highly efficient thermal interface materials," *Nano Lett.* **12**, 861 (2012).

<sup>2</sup>X. Zhao, Q. H. Zhang, D. J. Chen, and P. Lu, "Enhanced mechanical properties of graphene-based polyvinyl alcohol composites," *Macromolecules* **43**, 2357–2363 (2010).

<sup>3</sup>C. Kim, J.-M. Song, J.-S. Lee, and M. J. Lee, "All-solution-processed non-volatile flexible nano-floating gate memory devices," *Nanotechnology* **25**, 014016 (2014).

<sup>4</sup>N. Kang and S. I. Khondaker, "The impact of carbon sp<sup>2</sup> fraction of reduced graphene oxide on the performance of reduced graphene oxide contacted organic transistors," *Appl. Phys. Lett.* **105**, 223301 (2014).

<sup>5</sup>G. Khurana, P. Misra, and R. S. Katiyar, "Multilevel resistive memory switching in graphene sandwiched organic polymer heterostructure," *Carbon* **76**, 341–347 (2014).

<sup>6</sup>N. Yousefi, X. Sun, X. Lin, X. Shen, J. Jia, B. Zhang, B. Tang, M. Chan, and J. K. Kim, "Highly aligned graphene/polymer nanocomposites with excellent dielectric properties for high-performance electromagnetic interference shielding," *Adv. Mater.* **26**, 5480–5487 (2014).

<sup>7</sup>A. Rani, J.-M. Song, M. J. Lee, and J.-S. Lee, "Memory devices reduced graphene oxide based flexible organic charge trap memory devices," *Appl. Phys. Lett.* **101**, 233308 (2012).

<sup>8</sup>Y. Ji, M. Choe, B. Cho, S. Song, J. Yoon, H. C. Ko, and T. Lee, "Organic nonvolatile memory devices with charge trapping multilayer graphene film," *Nanotechnology* **23**, 105202 (2012).

<sup>9</sup>S. Stankovich, D. A. Dikin, G. H. B. Dommett, K. M. Kohlhaas, E. J. Zimney, E. A. Stach, R. D. Piner, S. B. T. Nguyen, and R. S. Ruoff, "Graphene-based composite materials," *Nature* **442**, 282–286 (2006).

<sup>10</sup>J. Du, L. Zhao, Y. Zeng, L. Zhang, F. Li, P. Liu, and C. Liu, "Comparison of electrical properties between multi-walled carbon nanotube and graphene nanosheet/high density polyethylene composites with a segregated network structure," *Carbon* **49**, 1094–1100 (2011).

<sup>11</sup>R. Islam, R. Chan-Yu-King, J.-F. Brun, C. Gors, A. Addad, M. Depriester, A. Hadj-Sahraoui, and F. Roussel, "Transport and thermoelectric properties of polyaniline/reduced graphene oxide nanocomposites," *Nanotechnology* **25**, 475705 (2014).

<sup>12</sup>The Graftity software is available at <http://www.graftitylabs.com>.

<sup>13</sup>The FOCUS software is available at [www.cemhti.cnrs-orleans.fr/pot/soft-ware/focus.html](http://www.cemhti.cnrs-orleans.fr/pot/soft-ware/focus.html).

<sup>14</sup>S. Quillard, G. Louarn, S. Lefrant, and A. G. MacDiarmid, "Vibrational analysis of polyaniline: A comparative study of leucoemeraldine, emeraldine, and pernigraniline bases," *Phys. Rev. B* **50**, 12496 (1994).

<sup>15</sup>R. Chan Yu King, F. Roussel, J.-F. Brun, and C. Gors, "Carbon nanotube polyaniline nanohybrids: Influence of the carbon nanotube characteristics on the morphological, spectroscopic, electrical and thermoelectric properties," *Synth. Met.* **162**, 1348–1356 (2012).

<sup>16</sup>R. Hawaldar, P. Merino, M. R. Correia, I. Bdkin, J. Gracio, J. Mendez, J. A. Martin-Gago, and M. K. Singh, "Large-area high-throughput synthesis of monolayer graphene sheet by hot filament thermal chemical vapor deposition," *Sci. Rep.* **2**, 682 (2012).

<sup>17</sup>M. Kim, C. Lee, and J. Jang, "Fabrication of highly flexible, scalable, and high-performance supercapacitors using polyaniline/reduced graphene oxide film with enhanced electrical conductivity and crystallinity," *Adv. Funct. Mater.* **24**, 2489–2499 (2014).

<sup>18</sup>A. N. Papanthanasios, I. Sakellis, and J. Grammatikakis, "Universal frequency-dependent ac conductivity of conducting polymer networks," *Appl. Phys. Lett.* **91**, 122911 (2007).

<sup>19</sup>A. N. Papanthanasios, I. Sakellis, J. Grammatikakis, E. Vitoratos, and S. Sakkopoulos, *Appl. Phys. Lett.* **103**, 123304 (2013).

<sup>20</sup>R. Kohlrausch, *Prog. Ann. Phys. Chem.* **72**, 393 (1847).

<sup>21</sup>G. Williams and D. C. Watts, "Non-symmetrical dielectric relaxation behaviour arising from a simple empirical decay function," *Trans. Faraday Soc.* **66**, 80 (1970).

<sup>22</sup>X. Tian, M. E. Itkis, E. B. Bekyarova, and R. C. Haddon, "Anisotropic thermal and electrical properties of thin thermal interface layers of graphite nanoplatelet-based composites," *Sci. Rep.* **3**, 1710 (2013).

<sup>23</sup>B. Marinho, M. Ghislandia, E. Tkalyac, C. E. Koning, and G. de With, "Electrical conductivity of compacts of graphene, multi-wall carbon nanotubes, carbon black, and graphite powder," *Powder Technol.* **221**, 351–358 (2012).

<sup>24</sup>L. K. H. van Beek, "Dielectric behavior of heterogeneous systems," in *Progress in Dielectrics*, edited by J. B. Birks (Heywood, London, 1967), Vol. 7, p. 69, pp.71–114.

<sup>25</sup>C. P. Lindsey and G. D. Patterson, "Detailed comparison of the Williams-Watts and Cole-Davidson functions," *J. Chem. Phys.* **73**(7), 3348 (1980).

<sup>26</sup>J. L. Barton, *Verres Ref.* **20**, 328 (1966); T. Nakajima, in *Annual Report on Conference on Electric Insulation and Dielectric Phenomena* (National Academy of Sciences, Washington, DC, 1972), pp. 168–176; H. Namikawa, *J. Non-Cryst. Solids* **18**, 173 (1975).